Observing photonic de Broglie waves without the maximally-path-entangled $|N,0\rangle + |0,N\rangle$ state

Osung Kwon, Young-Sik Ra, and Yoon-Ho Kim*

Department of Physics, Pohang University of Science and Technology (POSTECH), Pohang 790-784, Korea

(Received 30 June 2009; revised manuscript received 23 February 2010; published 1 June 2010)

The photonic de Broglie wave, in which an ensemble of N identical photons with wavelength λ reveals λ/N interference fringes, has been known to be a unique feature exhibited by the photon-number-path–entangled $|N,0\rangle + |0,N\rangle$ state or the $N00N$ state. Here, we report the observation of the photonic de Broglie wave for a pair of photons, generated by spontaneous parametric down-conversion, that are not photon-number-path entangled. We also show that the photonic de Broglie wave can even be observed for a pair of photons that are completely separable (i.e., no entanglement in all degrees of freedom) and distinguishable. The experimental and theoretical results suggest that the photonic de Broglie wave is, in fact, not related to the entanglement of the photons, rather it is related to the indistinguishable pathways established by the measurement scheme. The phase sensitivity surpassing the standard quantum limit, however, is shown to be closely related to the $N00N$ state.

DOI: 10.1103/PhysRevA.81.063801 PACS number(s): 42.50.Dv, 42.50.Ex, 42.65.Lm

I. INTRODUCTION

The nature of multipartite quantum entanglement is often manifested in quantum interference experiments. For example, in the case of entangled photon states generated by spontaneous parametric down-conversion (SPDC), quantum interference is observed in coincidence counts between two detectors, each individually exhibiting no interference fringes [1–3].

One notable example of photonic quantum interference is the photonic de Broglie wave in which an ensemble of N identical photons with wavelength λ exhibits λ/N interference fringes [4]. The photonic de Broglie wavelength λ/N can be observed at the N-photon detector placed at an output port of an interferometer if the beam splitters that make up the interferometer do not randomly split N photons. The quantum state of the photons in the interferometer is then the photon-number-path–entangled state or the $N00N$ state,

$$|\psi\rangle = (|N\rangle_1|0\rangle_2 + |0\rangle_1|N\rangle_2)/\sqrt{2}, \quad (1)$$

where the subscripts refer to the two interferometric paths. For this reason, the photonic de Broglie wave has been considered to be a unique feature exhibited by the $N00N$ state and essential for quantum imaging and quantum metrology [5–7]. Experimentally, photonic de Broglie waves up to $N = 4$ have been observed with corresponding $N00N$ states [8–12].

Note, however, that λ/N modulations in the coincidence rate among N detectors may not necessarily be of quantum origin. For instance, consider the λ/N modulation in coincidences among N detectors reported in Ref. [13], where each detector was placed at an output port of a multipath interferometer. The λ/N modulation in this case is a classical effect since the coincidence modulation is a direct result of modulations (with different phases) observed at individual detectors. This classical interference effect can be observed both with classical light (e.g., laser) and with nonclassical light. Also, classical thermal light may exhibit subwavelength interference fringes in coincidences but at the reduced visibility consistent with classical states [14,15]. Thus, the reduced-period fringe itself need not be of quantum origin. It is, however, important to point out that Nth order quantum interference, such as quantum optical λ/N modulations due to the photonic de Broglie wave, must exhibit high visibility (up to 100% in principle) in the absence of any lower-order interference. For example, it should not be possible to explain the second-order *quantum interference* effect with various first-order interference effects.

In this paper, we report an intriguing new observation of λ/N ($N = 2$) photonic de Broglie wave interference that has no classical interpretation and is not associated with the $N00N$ state. We also show theoretically that photonic de Broglie waves can even be observed for a pair of nonclassical single photons that are completely separable (i.e., no entanglement in all degrees of freedom) and distinguishable. The experimental and theoretical results suggest that the photonic de Broglie wave interference is, in fact, not related to the entanglement of the photons, rather it reflects the characteristics (i.e., the indistinguishable pathways) of the measurement scheme. The interferometric phase sensitivity surpassing the standard quantum limit, however, is shown to be closely related to the $N00N$ state.

II. PHOTONIC DE BROGLIE WAVE INTERFERENCE WITHOUT THE $N00N$ STATE: EXPERIMENT

Consider the experimental setup shown in Fig. 1. A 405-nm blue diode laser, with the full width at half-maximum (FWHM) bandwidth of 0.67 nm, pumps a 3-mm-thick type-I BBO crystal to generate, via the SPDC process, a pair of energy time-entangled photons centered at $\lambda = 810$ nm. The photon pair is coupled into the single-mode optical fiber after passing through the interference filter with an FWHM bandwidth of 5 nm. For optimal coupling, the pump was focused at the BBO and the focal spot was imaged to the single-mode fiber [16].

The photon pair is then sent to a Mach-Zehnder interferometer (MZI), formed with BS1 and BS2, via the different input ports a and b. The input delay x_1 between the photons is controlled by axially moving the output collimator of a fiber and the interferometer pathlength difference x_2 is controlled by translating one of the trombone prisms P2. A two-photon detector, consisting of BS3 and two single-photon detectors D3 and D4, is placed at the output mode e of MZI for photonic

*yoonho72@gmail.com

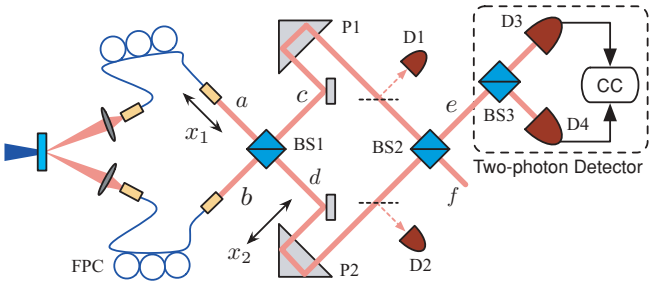

FIG. 1. (Color online) Schematic of the experiment. BS1, BS2, and BS3 are 50:50 beam splitters. FPC is the fiber polarization controller and CC is a coincidence counter.

de Broglie wave measurement [9]. Two auxiliary detectors, D1 and D2, are used to adjust the input delay x_1 by observing the Hong-Ou-Mandel (HOM) interference [17].

First, we consider the well-known photonic de Broglie wave for a biphoton $N00N$ state and this requires preparing the state $|\psi\rangle = (|2\rangle_c|0\rangle_d + |0\rangle_c|2\rangle_d)/\sqrt{2}$ in the MZI [4,9]. This can be accomplished by using HOM interference: the photon pair arrives at BS1 (or enters the MZI) simultaneously via the different input ports a and b. The high-visibility HOM interference, measured in coincidence counts between D1 and D2 as a function of x_1, reported in Fig. 2 indicates that when the input delay is zero (i.e., $x_1 = 0$), the quantum state of the photons in the interferometer is indeed the desired biphoton $N00N$ state.

Observation of the photonic de Broglie wave for the biphoton $N00N$ state requires: (i) interfering the biphoton amplitudes $|2\rangle_c|0\rangle_d$ and $|0\rangle_c|2\rangle_d$ and (ii) making a proper two-photon detection. In the experiment, we set $x_1 = 0$ with the help of the HOM dip in Fig. 2 and the photonic de Broglie wave corresponding to the biphoton $N00N$ state was observed at the two-photon detector placed at the output mode e of the MZI. The result shown in Fig. 3(a) exhibits $\lambda/2$ interference fringes as a function of the MZI pathlength difference x_2.

We note that the coincidence between single-photon detectors placed at modes e and f also exhibits the interference fringes with the period $\lambda/2$ [1,2]. This $\lambda/2$ interference fringe, however, is not related to the photonic de Broglie wave since (i) the photons are split at BS2 and (ii) it may be observed with

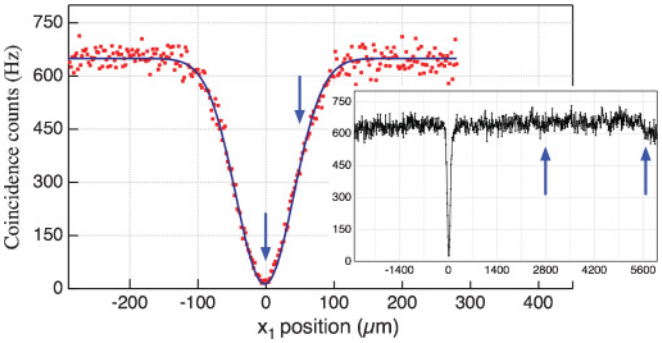

FIG. 2. (Color online) The Hong-Ou-Mandel dip observed with detectors D1 and D2. The dip visibility is better than 98%. The arrows represent the x_1 positions at which the biphoton interference measurements were performed with the two-photon detector (i.e., coincidences between detectors D3 and D4).

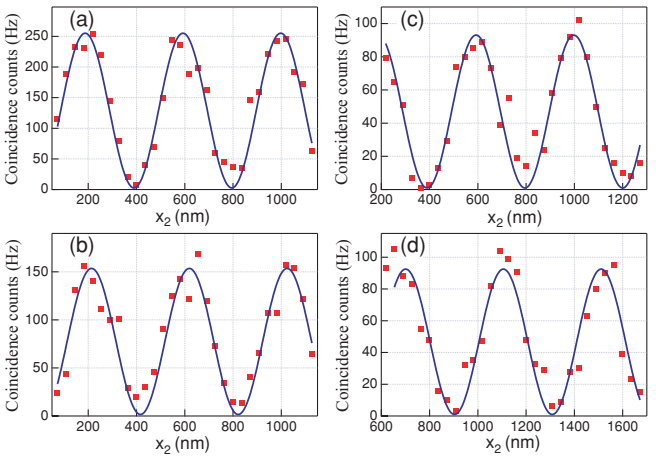

FIG. 3. (Color online) Biphoton interference observed at four different x_1 positions. (a) $x_1 = 0$ μm, (b) $x_1 = 62$ μm, (c) $x_1 = 2.8$ mm, (d) $x_1 = 5.7$ mm. The solid lines are fit to the data with the modulation wavelength and the visibility fixed at $\lambda/2 = 405$ nm and 98%, respectively.

the classical coherent state (e.g., $|0\rangle_a|\alpha\rangle_b$) at the input of the MZI [9,13].

Consider now the situation in which the photons do not enter the MZI simultaneously. In this case, since the photons do not arrive at BS1 at the same time, HOM interference does not occur and the quantum state of the photons in the MZI is no longer the biphoton $N00N$ state. The question we ask is whether the $\lambda/2$ photonic de Broglie wave would still be observed at the two-photon detector in mode e (i.e., coincidences between detectors D3 and D4) in this case.

To probe this question, we intentionally add more time delays in mode a of the MZI so that $x_1 \neq 0$. The arrows in Fig. 2 indicate the x_1 positions at which the biphoton interference measurements are made with the two-photon detector in mode e. First, we set $x_1 = 62$ μm and x_2 is scanned for the two-photon interference measurement. At this x_1 location, there is still some Hong-Ou-Mandel interference as evidenced in Fig. 2 (i.e., the coincidence rate is still below the random coincidence rate). The biphoton interference measured with the two-photon detector in this condition is shown in Fig. 3(b). Interestingly, the observed interference fringes exhibit the same $\lambda/2$ modulation with no reduction in visibility. It is intriguing to find that the same high-visibility interference fringes with $\lambda/2$ modulations are observed even when x_1 is completely out of the Hong-Ou-Mandel dip region. In Figs. 3(c) and 3(d), we show the biphoton interference observed with the two-photon detector at $x_1 = 2.8$ mm and at $x_1 = 5.7$ mm, respectively. These data correspond to the x_1 positions marked with the arrows shown in the inset of Fig. 2.

So far, we have established experimentally that the photonic de Broglie wave can indeed be observed without the $N00N$ state. (Note that, differently from Ref. [13], this is a real second-order quantum effect in the absence of any first-order interference: the detectors D3 and D4 individually do not show any modulations.) We now ask whether the shapes of the photonic de Broglie wave packets would remain the same. This question is probed by measuring the photonic de Broglie

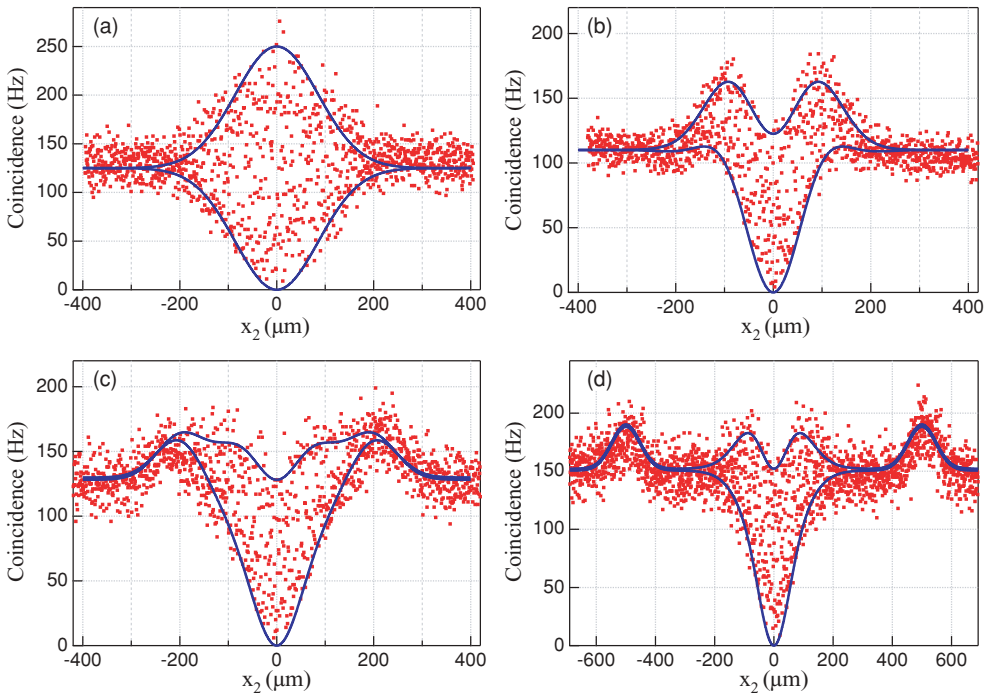

FIG. 4. (Color online) The biphoton wave-packet measurements with varying input delays at BS1. (a) $x_1 = 0$ μm, (b) $x_1 = 100$ μm, (c) $x_1 = 200$ μm, and (d) $x_1 = 500$ μm. Within the wave packets, the modulation period is $\lambda/2$ and the visibility around $x_2 = 0$ is better than 98%. The solid lines are the wave-packet envelopes calculated using Eq. (15).

wave packets for several different x_1 values and the results of these measurements are shown in Fig. 4 [18].

In Fig. 4(a), we show the typical symmetric Gaussian de Broglie wave packet for the biphoton $N00N$ state generated by setting $x_1 = 0$ μm. This case corresponds to Fig. 3(a). For non-$N00N$ states (i.e., for $x_1 \neq 0$), it is found that the photonic de Broglie wave packet is modified dramatically. The wave packet starts to become highly asymmetric (with respect to the random coincidence rate) as soon as $x_1 \neq 0$; see Fig. 4(b). The wave-packet envelope then takes the shape of a double hump and a single dip for a larger value of x_1; see Fig. 4(c). Eventually, for a sufficiently large x_1, small side peaks start to appear at $x_2 = \pm x_1$; see Fig. 4(d). Even for very large values of x_1 (e.g., corresponding to the positions marked with arrows in the inset of Fig. 2), the wave-packet shape remains essentially the same as in Fig. 4(d) but the two side peaks get relocated to their new positions, $x_2 = \pm x_1$ [18].

III. PHOTONIC DE BROGLIE WAVE INTERFERENCE WITHOUT THE $N00N$ STATE: THEORY

A. Theoretical description

To explain the observed phenomena theoretically, we start by writing the monochromatic laser-pumped SPDC two-photon state as [19]

$$|\psi\rangle_{\rm e} = \int d\omega_s d\omega_i\, \delta(\Delta_\omega)\mathrm{sinc}(\Delta_k L/2) e^{i\Delta_k L/2} |\omega_s, \omega_i\rangle, \qquad (2)$$

where the subscripts i, s, and p refer to the idler, the signal, and the pump photon, respectively. The thickness of the SPDC crystal is L, $\Delta_\omega = \omega_p - \omega_s - \omega_i$, and $\Delta_k = k_p - k_s - k_i$. Since the pump is a cw diode laser with a rather large FWHM bandwidth, the SPDC quantum state with a cw diode laser pump should more properly be written as [18]

$$\rho = \int d\omega_p\, \mathcal{S}(\omega_p) |\psi\rangle_{\rm ee}\langle\psi|, \qquad (3)$$

where the spectral power density of the pump is assumed to be Gaussian,

$$\mathcal{S}(\omega_p) \equiv \exp[-(\omega_p - \omega_{p0})^2/2\Delta{\omega_p}^2]/\Delta\omega_p\sqrt{2\pi}, \qquad (4)$$

such that $\int \mathcal{S}(\omega_p) d\omega_p = 1$.

The HOM interference can be calculated by evaluating

$$R_{12} = \int dt dt'\, \mathrm{tr}[\rho\, E_c^{(-)}(t) E_d^{(-)}(t') E_d^{(+)}(t') E_c^{(+)}(t)], \qquad (5)$$

where

$$E_c^{(+)}(t) = [i E_a^{(+)}(t - \tau_1) + E_b^{(+)}(t)]/\sqrt{2}, \qquad (6)$$

$$E_d^{(+)}(t) = [E_a^{(+)}(t - \tau_1) + i E_b^{(+)}(t)]/\sqrt{2}, \qquad (7)$$

and $\tau_1 = x_1/c$. The positive frequency component of the electric field in mode a is given as

$$E_a^{(+)}(t) = \int d\omega\, a(\omega)\phi(\omega) e^{-i\omega t}, \qquad (8)$$

where $a(\omega)$ is the annihilation operator for the signal photon in mode a and $E_b^{(+)}(t)$ for the idler photon in mode b is similarly defined. The filter transmission is assumed Gaussian,

$$\phi(\omega) = \exp[-(\omega - \omega_0)^2/2\Delta\omega^2]/\sqrt{\Delta\omega\sqrt{\pi}}, \qquad (9)$$

and $\int |\phi(\omega)|^2 d\omega = 1$. Since the natural bandwidth of SPDC, $\mathrm{sinc}(\Delta_k L/2)$, is much broader than the spectral filter bandwidth $\Delta\omega$, Eq. (5) is calculated to be

$$R_{12} = 1 - \exp\left(-\Delta\omega^2 \tau_1^2/2\right). \tag{10}$$

The solid line in Fig. 2 is plotted using Eq. (10) with measured spectral filter bandwidth $\Delta\omega$.

For the photonic de Broglie wave measurement, the response of the two-photon detector in mode e must be considered and it is given as

$$R_{ee} = \int dt dt'\, tr[\rho\, E_e^{(-)}(t) E_e^{(-)}(t') E_e^{(+)}(t') E_e^{(+)}(t)], \tag{11}$$

where

$$E_e^{(+)}(t) = [i E_c^{(+)}(t) + E_d^{(+)}(t - \tau_2)]/\sqrt{2}, \tag{12}$$

and $\tau_2 = x_2/c$. Equation (11) can then be rewritten as

$$R_{ee} = \int d\omega_p \mathcal{S}(\omega_p) \int dt dt'\, |\langle 0| E_e^{(+)}(t') E_e^{(+)}(t) |\psi\rangle_{\mathrm{e}}|^2, \tag{13}$$

where $\langle 0|$ denotes the vacuum state. The biphoton amplitude $\langle 0| E_e^{(+)}(t') E_e^{(+)}(t) |\psi\rangle_{\mathrm{e}}$ contains important information about the quantum interference and, when expanded using the electric field operators at input modes a and b, is calculated to be

$$\begin{aligned}
&\langle 0| E_e^{(+)}(t') E_e^{(+)}(t) |\psi\rangle_{\mathrm{e}} \\
&= \frac{i}{4} \langle 0| [E_a^{(+)}(t - \tau_1 - \tau_2) E_b^{(+)}(t' - \tau_2) \\
&\quad + E_a^{(+)}(t' - \tau_1 - \tau_2) E_b^{(+)}(t - \tau_2) - E_a^{(+)}(t - \tau_1) E_b^{(+)}(t') \\
&\quad - E_a^{(+)}(t' - \tau_1) E_b^{(+)}(t) - E_a^{(+)}(t - \tau_1) E_b^{(+)}(t' - \tau_2) \\
&\quad - E_a^{(+)}(t' - \tau_1) E_b^{(+)}(t - \tau_2) + E_a^{(+)}(t - \tau_1 - \tau_2) E_b^{(+)}(t') \\
&\quad + E_a^{(+)}(t' - \tau_1 - \tau_2) E_b^{(+)}(t)] |\psi\rangle_{\mathrm{e}}.
\end{aligned} \tag{14}$$

Note that only nonzero biphoton amplitudes are written in the above equation: terms that contain $E_a^{(+)} E_a^{(+)}$ and $E_b^{(+)} E_b^{(+)}$ are eventually calculated to be zero because of the nature of the input state $|\psi\rangle_{\mathrm{e}}$.

If we now consider the two-photon detector shown in Fig. 1, the normalized coincidence rate between detectors D3 and D4 corresponds to R_{ee} and is given as

$$\begin{aligned}
R_{34} = \tfrac{1}{4}\{&4 + \exp[-(\tau_1 - \tau_2)^2 \Delta\omega^2/2] \\
&+ \exp[-(\tau_1 + \tau_2)^2 \Delta\omega^2/2] - 2\exp\left(-\tau_2^2 \Delta\omega^2/2\right) \\
&- 2\cos(2\omega_0 \tau_2) \exp\left(-\tau_2^2 \Delta\omega_e^2/2\right) \\
&\times \left[1 + \exp\left(-\tau_1^2 \Delta\omega^2/2\right)\right]\},
\end{aligned} \tag{15}$$

where $1/\Delta\omega_e^2 \equiv 1/\Delta\omega_p^2 + 1/\Delta\omega^2$.

Equation (15) clearly shows that the $2\omega_0$ or $\lambda_0/2$ interference fringe (corresponding to the photonic de Broglie wavelength), in fact, is not related to the biphoton $N00N$-state condition $\tau_1 = 0$. As long as τ_2 is within the effective coherence length $\sqrt{2}/\Delta\omega_e$, the biphoton photonic de Broglie wave interference can be observed regardless of the τ_1 value.

Another interesting feature of Eq. (15) is that the shape of the biphoton de Broglie wave packet is τ_1 dependent while the period of interference fringes remains the same at $2\omega_0$. Note also that the maximum interference visibility is not affected by τ_1. The theoretical result in Eq. (15) is found to be in excellent agreement with the experimental data in Fig. 4.

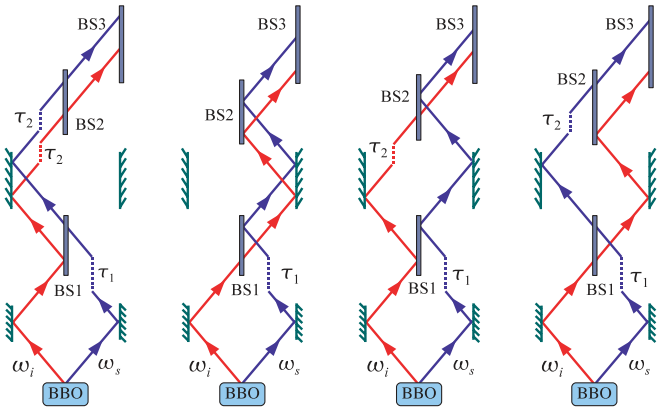

FIG. 5. (Color online) The Feynman paths for the photon pair. All the Feynman paths become indistinguishable when $\tau_2 = 0$, regardless of τ_1 values. Note that each line (top to bottom) in Eq. (14) corresponds to each Feynman path (left to right).

B. The Feynman diagram

The interesting features of the biphoton de Broglie interference in this experiment can be intuitively understood by analyzing the Feynman diagrams representing the two-photon detection amplitudes.

Given the experimental setup in Fig. 1, there exist four Feynman paths in which the photon pair exits BS2 via the output mode e and these Feynman paths are shown in Fig. 5. Since the signal, ω_s, and idler, ω_i, photons must always transmit (reflect) and reflect (transmit) at BS3 to contribute to a final two-photon detection event, each Feynman path shown in Fig. 5 branches off into two final Feynman amplitudes. There are, thus, a total of eight Feynman paths which lead to a detection event at the two-photon detector in Fig. 1.

The photonic de Broglie wavelength observed in Fig. 3 is a manifestation of quantum interference among these Feynman paths. For arbitrary τ_1 and τ_2, the Feynman paths shown in Fig. 5 are clearly distinguishable (in time). However, if $\tau_2 = 0$, all Feynman paths become indistinguishable, regardless of τ_1 values. This is confirmed theoretically in Eq. (15) and experimentally in Fig. 3: high-visibility $2\omega_0$ or $\lambda/2$ interference fringes are observed when τ_2 is scanned around $\tau_2 = 0$.

In addition, it is shown in Fig. 4 that the shape of the biphoton wave packet is dependent on the τ_1 value. In the case that $\tau_1 = 0$, the third and fourth Feynman paths in Fig. 5 cancel out and the wave-packet envelope is determined by the overlap between the first two Feynman paths. As shown in Fig. 4(a), the result is a Gaussian wave packet whose width is determined by $\Delta\omega_e$.

Consider now the case of $\tau_2 = \tau_1$. The signal and idler photons arrive simultaneously at BS2 for the third Feynman path in Fig. 5 and, because of the Hong-Ou-Mandel effect, the two photons will always exit BS2 via the same output port. If we now consider the case of $\tau_2 = -\tau_1$, the same situation

occurs for the fourth Feynman path in Fig. 5. Therefore, the detection probability of the third and the fourth Feynman paths would increase twice as big compared to $\tau_2 \neq \pm\tau_1$. The net results are the distinct side peaks observed at $\tau_2 = \pm\tau_1$ in Fig. 4(d).

In general (i.e., $\tau_1 \neq 0$), all the eight Feynman paths contribute to quantum interference in a complex manner so an intuitive explanation becomes difficult.

IV. PHASE SENSITIVITY

In Secs. II and III, we have shown both in experiment and in theory that the photonic de Broglie wave interference can be observed without the *N*00*N* state. In other words, the so-called *phase superresolution* can be achieved without using the photonic *N*00*N* state. Note that, since high-visibility two-photon interference exhibiting the fringe spacing of $\lambda/2$ is observed without any first-order interference, this is a genuine quantum interference effect, different from the classical effect shown in Ref. [13].

In this section, we consider the question of phase sensitivity of our quantum interferometer. Specifically, we explore whether the so-called *phase supersensitivity* can be achieved without the *N*00*N* state. The phase sensitivity $\mathcal{S}$ in an N-photon interferometer can be defined as the ratio of the phase error in the interferometer under study and the phase error at the standard quantum limit (SQL) [20]. If we choose an optimal value of the bias phase for the two-photon interferometer ($N = 2$), the maximum phase sensitivity, $\mathcal{S}_M$ is found to be [20]

$$2\mathcal{S}_M^{-2} = 1 + \frac{(1-\eta)^2/\eta}{1 - \frac{\eta}{2} - \frac{\eta V^2}{2} - \sqrt{(1-V^2)\left[\left(1-\frac{\eta}{2}\right)^2 - \left(\frac{\eta V}{2}\right)^2\right]}}, \tag{16}$$

where η is the intrinsic detection efficiency and V is the fringe visibility. At SQL, $\mathcal{S}_M = 1$ and $\mathcal{S}_M > 1$ corresponds to *phase supersensitivity*.

We have calculated the maximum phase sensitivity $\mathcal{S}_M$ from the experimental data shown in Figs. 3 and 4 and the results are shown in Fig. 6. The condition $x_1 = 0$ μm corresponds to the *N*00*N* state condition and, as seen in Fig. 4, changes in the x_1 value cause significant reshaping of the wave packet which in turn affects the value of η. The value η is calculated from the experimental data as the ratio between the maximum coincidence count rate at $x_2 \approx 0$ μm (the visibility is highest at this point) and twice the random coincidence rate. Different η values then correspond to different values of x_1.

Figure 6 shows a few interesting characteristics. When $V = 1$, the *N*00*N* state condition ($x_1 = 0$ μm) leads to the Heisenberg-limited phase supersensitivity of $\mathcal{S}_M = \sqrt{2}$. For non-*N*00*N* states (e.g., $x_1 > 150$ μm), SQL ($\mathcal{S}_M = 1$) can still be reached. If the visibility is lower, the phase sensitivity is accordingly reduced and it can be seen in Fig. 6 that, with $V = 0.98$, it is not even possible to reach SQL if *N*00*N* states are not used. It is interesting to note that nonperfect *N*00*N* states (e.g., $x_1 < 100$ μm) also exhibit phase supersensitivity.

We can therefore conclude that, even in quantum interferometry, phase supersensitivity requires a particular entangled state or the *N*00*N* state in the interfrometer while phase superresolution can be achieved with non-*N*00*N* states.

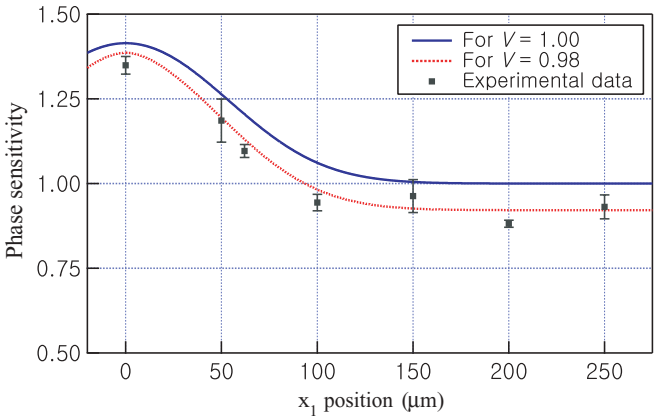

FIG. 6. (Color online) Maximum phase sensitivity $\mathcal{S}_M$ at different x_1 positions. The solid and dotted lines are calculated from Eq. (16) for $V = 1.00$ and $V = 0.98$, respectively. Phase sensitivity greater than 1 corresponds to phase supersensitivity (i.e., phase sensitivity better than SQL). The Heisenberg limit $\mathcal{S}_M = \sqrt{2}$ is reached at $x_1 = 0$ μm and at $V = 1.00$, corresponding to a perfect two-photon *N*00*N* state. For non-*N*00*N* states (e.g., $x_1 > 150$ μm), SQL ($\mathcal{S}_M = 1$) is reached for $V = 1.00$. It is interesting to note that nonperfect *N*00*N* states also exhibit phase supersensitivity.

V. PHOTONIC DE BROGLIE WAVE INTERFERENCE WITH NONENTANGLED PHOTON PAIRS

So far, we have shown experimentally and theoretically that the photonic de Broglie wave is in fact not related to the photon-number-path–entangled or the *N*00*N* state. The photonic de Broglie wave, instead, appears to be linked to the underlying spectral entanglement of SPDC photons which are used for both experimental observation and theoretical analysis [19]. The question then becomes whether the two input photons need to have any entanglement at all to exhibit the photonic de Broglie wave phenomenon.

A. Photonic de Broglie wave interference for two identical photons with no entanglement

Consider two single photons with identical spectra and polarization, each emitted from a separate single-photon source. It is known that HOM interference can occur with a pair of identical single photons [21,22]. The biphoton *N*00*N* state resulting from HOM interference should then exhibit the photonic de Broglie wave.

The relevant question therefore is what would happen when there is no HOM interference between the two identical single photons with no *a priori* entanglement. Would the photonic de Broglie wave still be observed in the absence of any entanglement between the photons?

To investigate this question, let us consider a single photon in the pure state at each input mode of the MZI in Fig. 1. Since the joint quantum state of the two single photons at the input modes of the MZI is separable, it can be written as

$$|\psi\rangle_s = \int d\omega_a\, \varphi(\omega_a)|\omega_a\rangle \otimes \int d\omega_b\, \varphi(\omega_b)|\omega_b\rangle, \tag{17}$$

where the single-photon spectral amplitude is assumed to be Gaussian,

$$\varphi(\omega) = \exp[-(\omega-\omega_0)^2/2\Delta\omega^2]/\sqrt{\Delta\omega\sqrt{\pi}}, \qquad (18)$$

and $\int |\varphi(\omega)|^2 d\omega = 1$.

Given the input quantum state as in Eq. (17), the response of the MZI can now be studied. First, the single-photon detection rates at D3 and D4 are calculated to be constant, completely independent of x_1 and x_2. This is because the single-photon detection probabilities due to the single photons in mode a and in mode b have the same Gaussian envelopes but are out of phase by 180°. In other words, similarly to the case of entangled-photon pairs at the input, no first-order interference can be observed. Second, the two-photon detection rates for the photonic de Broglie wave measurement can be calculated by evaluating

$$R_{ee}^{(s)} = \int dt dt' \, tr[\rho^{(s)} E_e^{(-)}(t) E_e^{(-)}(t') E_e^{(+)}(t') E_e^{(+)}(t)], \qquad (19)$$

where $\rho^{(s)} = |\psi\rangle_{ss}\langle\psi|$. The above equation can then be rewritten as

$$R_{ee}^{(s)} = \int dt dt' \, |\langle 0|E_e^{(+)}(t') E_e^{(+)}(t)|\psi\rangle_s|^2. \qquad (20)$$

The biphoton amplitude $\langle 0|E_e^{(+)}(t')E_e^{(+)}(t)|\psi\rangle_s$ in Eq. (20) is evaluated to be

$$\begin{aligned}
&\langle 0|E_e^{(+)}(t')E_e^{(+)}(t)|\psi\rangle_s \\
&= \frac{i}{4}\langle 0|[E_a^{(+)}(t-\tau_1-\tau_2)E_b^{(+)}(t'-\tau_2) \\
&\quad + E_a^{(+)}(t'-\tau_1-\tau_2)E_b^{(+)}(t-\tau_2) - E_a^{(+)}(t-\tau_1)E_b^{(+)}(t') \\
&\quad - E_a^{(+)}(t'-\tau_1)E_b^{(+)}(t) - E_a^{(+)}(t-\tau_1)E_b^{(+)}(t'-\tau_2) \\
&\quad - E_a^{(+)}(t'-\tau_1)E_b^{(+)}(t-\tau_2) + E_a^{(+)}(t-\tau_1-\tau_2)E_b^{(+)}(t') \\
&\quad + E_a^{(+)}(t'-\tau_1-\tau_2)E_b^{(+)}(t)]|\psi\rangle_s. \qquad (21)
\end{aligned}$$

Finally, the normalized coincidence rate on D3 and D4 in Fig. 1 is proportional to $R_{ee}^{(s)}$ and is given as

$$\begin{aligned}
R_{34}^{(s)} &= \tfrac{1}{4}\{4 + \exp[-(\tau_1-\tau_2)^2\Delta\omega^2/2] \\
&\quad + \exp[-(\tau_1+\tau_2)^2\Delta\omega^2/2] - 2\exp(-\tau_2^2\Delta\omega^2/2) \\
&\quad - 2\cos(2\omega_0\tau_2)\exp\left(-\tau_2^2\Delta\omega^2/2\right) \\
&\quad \times \left[1 + \exp\left(-\tau_1^2\Delta\omega^2/2\right)\right]\}. \qquad (22)
\end{aligned}$$

It is interesting to note that the result in Eq. (22) is identical to Eq. (15) but with $\Delta\omega_e$ replaced by $\Delta\omega$. Effectively, this means that SPDC pumped with a very broadband pump laser would give the identical result as that of two separable single-photon states. The theoretical results summarized in Fig. 7 show that the separable two-photon state of Eq. (17) at the input of the MZI gives nearly the same result as that of SPDC photons pumped with a laser with 2-nm FWHM bandwidth for both the $N00N$ state ($x_1 = 0$ μm) and non-$N00N$ state ($x_1 \neq 0$ μm) conditions.

B. Photonic de Broglie wave interference for two distinguishable (orthogonally polarized) photons with no entanglement

In the previous section, we have seen that entanglement is in fact not necessary for observing the photonic de Broglie wave interference of two photons. It was, however, assumed that the two input single photons were identical. In this section, we discuss the general case in which the two input single photons are orthogonally polarized so that they are completely distinguishable. Note that the experimental schematic is kept the same as in Fig. 1: no polarization-information-erasing polarizers are added to the setup.

For two orthogonally polarized single photons, the joint quantum state is written as

$$|\psi\rangle_{dist} = \int d\omega_a \, \phi(\omega_a)|\omega_a^H\rangle \otimes \int d\omega_b \, \phi(\omega_b)|\omega_b^V\rangle, \qquad (23)$$

where the superscripts H and V refer to horizontal and vertical polarization states, respectively. The counting rate at the two-photon detector (see Fig. 1) in the output mode e of BS2 is then given as

$$\begin{aligned}
R_{ee}^{(dist)} &= \sum_{p_1,p_2\in\{H,V\}} \int dt dt' \, tr\left[\rho^{(dist)} E_e^{p_1(-)}(t) E_e^{p_2(-)}(t')\right. \\
&\quad \left. \times E_e^{p_2(+)}(t') E_e^{p_1(+)}(t)\right], \qquad (24)
\end{aligned}$$

where superscripts p_1 and p_2 denote polarizations and $\rho^{(dist)} = |\psi\rangle_{dist}\,{}_{dist}\langle\psi|$. Equation (24) can then be rewritten as

$$\begin{aligned}
R_{ee}^{(dist)} &= \int dt dt' \sum_{p_1,p_2\in\{H,V\}} \left|\langle 0|E_e^{p_2(+)}(t')E_e^{p_1(+)}(t)|\psi\rangle_{dist}\right|^2 \\
&= \int dt dt' \left(\left|\langle 0|E_e^{H(+)}(t')E_e^{V(+)}(t)|\psi\rangle_{dist}\right|^2\right. \\
&\quad \left. + \left|\langle 0|E_e^{V(+)}(t')E_e^{H(+)}(t)|\psi\rangle_{dist}\right|^2\right). \qquad (25)
\end{aligned}$$

Note that terms that include electric field operators $E_e^{H(+)}E_e^{H(+)}$ and $E_e^{V(+)}E_e^{V(+)}$ are not shown because they eventually are calculated to be zero since the input photons are orthogonally polarized.

The biphoton amplitudes are then expanded as

$$\begin{aligned}
&\langle 0|E_e^{H(+)}(t')E_e^{V(+)}(t)|\psi\rangle_{dist} \\
&= \frac{i}{4}\langle 0|\left[E_a^{H(+)}(t-\tau_1-\tau_2)E_b^{V(+)}(t'-\tau_2)\right. \\
&\quad - E_a^{H(+)}(t-\tau_1)E_b^{V(+)}(t') - E_a^{H(+)}(t-\tau_1)E_b^{V(+)}(t'-\tau_2) \\
&\quad \left. + E_a^{H(+)}(t-\tau_1-\tau_2)E_b^{V(+)}(t')\right]|\psi\rangle_{dist}, \qquad (26)
\end{aligned}$$

and

$$\begin{aligned}
&\langle 0|E_e^{V(+)}(t')E_e^{H(+)}(t)|\psi\rangle_{dist} \\
&= \frac{i}{4}\langle 0|\left[E_a^{H(+)}(t'-\tau_1-\tau_2)E_b^{V(+)}(t-\tau_2)\right. \\
&\quad - E_a^{H(+)}(t'-\tau_1)E_b^{V(+)}(t) - E_a^{H(+)}(t'-\tau_1)E_b^{V(+)}(t-\tau_2) \\
&\quad \left. + E_a^{H(+)}(t'-\tau_1-\tau_2)E_b^{V(+)}(t)\right]|\psi\rangle_{dist}. \qquad (27)
\end{aligned}$$

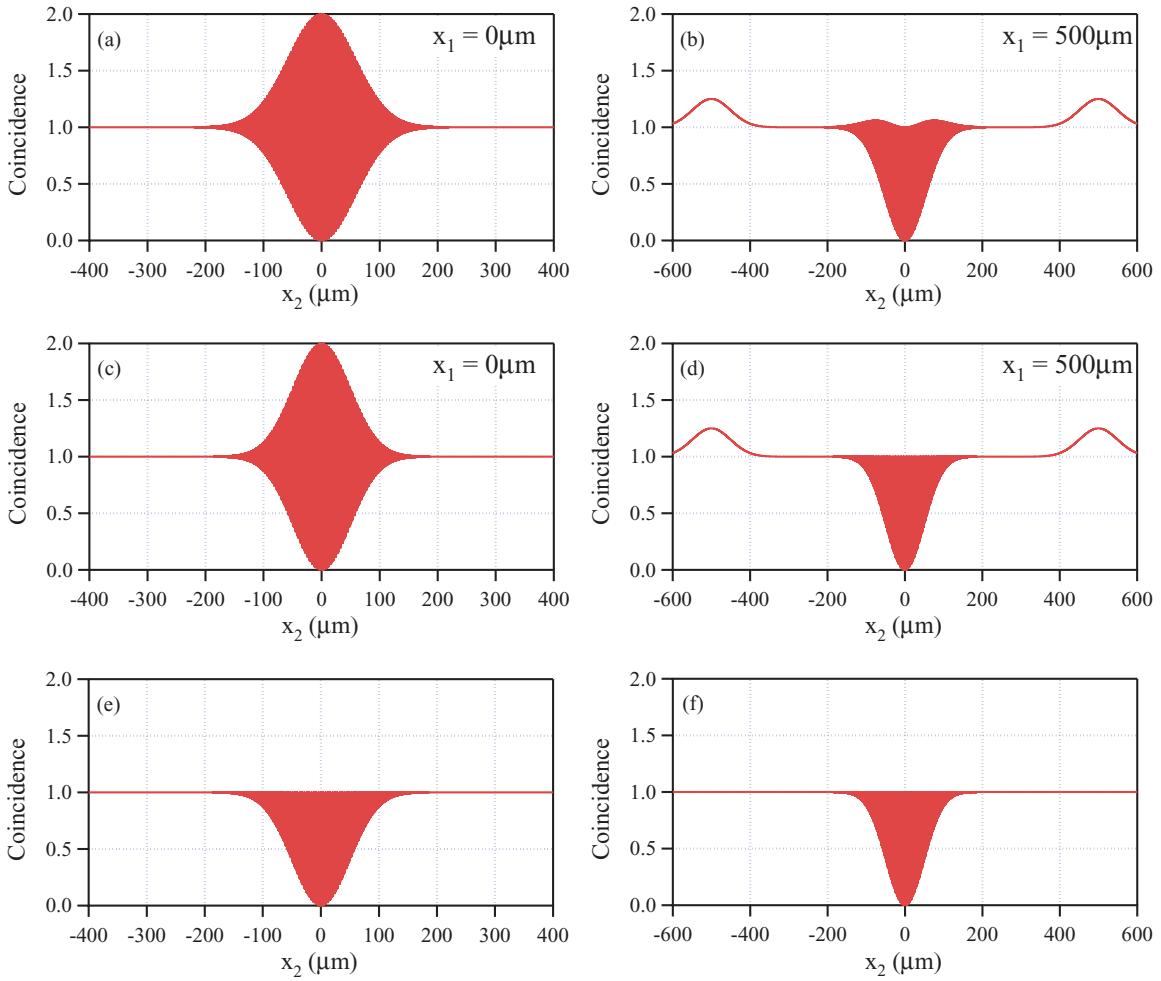

FIG. 7. (Color online) Calculated photonic de Broglie wave packets for SPDC photons (a) and (b); for two identical single photons with no entanglement (c) and (d); and for two distinguishable (orthogonally polarized) single photons with no entanglement (e) and (f). The plots (a) and (b), (c) and (d), and (e) and (f) are due to the theoretical results in Eqs. (15), (22), and (28), respectively. For SPDC photons, the pump bandwidth $\Delta\omega_p$ is assumed to be 2-nm FWHM and the signal and the idler photons are filtered with 5-nm FWHM filters. For single photons, they are assumed to have FWHM bandwidth of 5 nm. Note that, since Eq. (28) is τ_1 independent, (e) and (f) are identical plots with different ranges.

Finally, the normalized output of the two-photon detector (i.e., coincidence between D3 and D4) is calculated to be

$$R_{34}^{(\mathrm{dist})} = \tfrac{1}{4}\{4 - 2\exp\left(-\tau_2^2\Delta\omega^2/2\right) - 2\cos\left(2\omega_0\tau_2\right)\exp\left(-\tau_2^2\Delta\omega^2/2\right)\}. \quad (28)$$

It is interesting to note that Eq. (28) also shows $2\omega_0$ modulation as in the case of two identical single photons [Eq. (22)], and as in the case of a pair of SPDC photons [Eq. (15)]. This result, therefore, reveals that photonic de Broglie wave interference is not only unrelated to the $N00N$ state, but it can also be observed with completely unentangled and distinguishable photons. Note also that Eq. (28) is completely independent of τ_1 and Eq. (28) can actually be obtained from Eq. (22) by letting $\tau_1 \to \infty$.

Equation (28) is plotted in Figs. 7(e) and 7(f). The plots show very clearly that high-visibility photonic de Broglie wave interference appear for two orthogonally polarized single photons. Note, however, that the shape of the wave packet in Fig. 7(e) is quite different from Figs. 7(a) and 7(c) but rather similar to Figs. 7(b) and 7(d). This comes from the fact that Eq. (28) is τ_1 independent and the other two results converge toward Eq. (28) as τ_1 gets bigger. This fact is also reflected in the absence of side peaks in Fig. 7(f).

We can now comment on phase sensitivity for interferograms shown in Fig. 7. Clearly, as we have discussed in Sec. IV, only Figs. 7(a) and 7(c) would lead to phase supersensitivity. (The visibility is 1 in all plots.) Since the phase supersensitivity conditions in Figs. 7(a) and 7(c) directly leads to the two-photon $N00N$ state in the interferometer and vice versa, the $N00N$ state interferometer is an essential tool in achieving phase supersensitivity. Phase superresolution, on the other hand, does not require $N00N$ states as witnessed in Fig. 7(e): two input single photons are orthogonally polarized so no $N00N$ states are formed in the interferometer, yet high-visibility $\lambda/2$ second-order interference fringes are observed without any first-order interference.

VI. SUMMARY

We have shown both in experiment and in theory that photonic de Broglie wave interference can be observed for non-*N*00*N* states as well as for *N*00*N* states using a pair of energy-time-entangled spontaneous parametric down-conversion photons. It is important to point out that both the *N*00*N* state interference and the non-*N*00*N* state interference demonstrated in this paper are quantum interference which cannot be observed with classical light: the coincidence events between two single-photon detectors exhibit the second-order modulations (interference) while the single-photon detection rates do not show any first-order interference fringes.

We then examined the connection between the photonic de Broglie wave interference and entanglement between the input single photons. The monochromatic-pumped SPDC in Eq. (2) is strongly energy-time-entangled and, as the pump bandwidth is increased, the degree of energy-time entanglement is reduced [23]. The experimental and theoretical results on photonic de Broglie wave interference for broadband-pumped SPDC shown in Figs. 4(d) and 7(b) make it clear that the quality of the photonic de Broglie wave interference for non-*N*00*N* states is not affected by the reduced energy-time entanglement between the photon pair at the input. Furthermore, Figs. 7(d) and 7(f) show that even two nonentangled and distinguishable (orthogonally polarized) single photons lead to essentially the same photonic de Broglie wave interference.

These results therefore reveal that entanglement between the two input photons plays essentially no role in the manifestation of the photonic de Broglie wave interference. Rather, it is the measurement scheme (i.e., indistinguishable pathways established by the measurement scheme) that brings out the photonic de Broglie wave phenomenon [24]. Note, again, that for observing quantum interference, the input photons are still required to be nonclassical (e.g., entangled SPDC photon pairs, two separable single-photon states, etc.).

Although the photonic de Broglie wave interference, which is linked to phase superresolution, has been shown to be unrelated to the *N*00*N* state, phase supersensitivity has been shown to be closely tied to the *N*00*N* state. We have shown that non-*N*00*N* states can only achieve phase sensitivity up to the standard quantum limit while *N*00*N* states can exhibit the Heisenberg-limited phase sensitivity. In experiment, *N*00*N* states and nonperfect *N*00*N* states are shown to exhibit phase supersensitivity while non-*N*00*N* states exhibit phase sensitivity less than the standard quantum limit.

The experimental and theoretical results in this paper apply to $N = 2$ photonic de Broglie wave interference. It will be an interesting problem to study these effects for the N-photon case.

ACKNOWLEDGMENTS

This work was supported, in part, by the National Research Foundation of Korea (Grant Nos. 2009-0070668 and 2009-0084473) and the Ministry of Knowledge and Economy of Korea through the Ultrafast Quantum Beam Facility Program.

[1] J. G. Rarity, P. R. Tapster, E. Jakeman, T. Larchuk, R. A. Campos, M. C. Teich, and B. E. A. Saleh, Phys. Rev. Lett. **65**, 1348 (1990).
[2] Z. Y. Ou, X. Y. Zou, L. J. Wang, and L. Mandel, Phys. Rev. A **42**, 2957 (1990).
[3] J. Brendel, E. Mohler, and W. Martienssen, Phys. Rev. Lett. **66**, 1142 (1991).
[4] J. Jacobson, G. Bjork, I. Chuang, and Y. Yamamoto, Phys. Rev. Lett. **74**, 4835 (1995).
[5] A. N. Boto, P. Kok, D. S. Abrams, S. L. Braunstein, C. P. Williams, and J. P. Dowling, Phys. Rev. Lett. **85**, 2733 (2000).
[6] M. D'Angelo, M. V. Chekhova, and Y. H. Shih, Phys. Rev. Lett. **87**, 013602 (2001).
[7] K. T. Kapale and J. P. Dowling, Phys. Rev. Lett. **99**, 053602 (2007).
[8] E. J. S. Fonseca, C. H. Monken, and S. Padua, Phys. Rev. Lett. **82**, 2868 (1999).
[9] K. Edamatsu, R. Shimizu, and T. Itoh, Phys. Rev. Lett. **89**, 213601 (2002).
[10] P. Walther, J.-W. Pan, M. Aspelmeyer, R. Ursin, S. Gasparoni, and A. Zeilinger, Nature **429**, 158 (2004).
[11] M. W. Mitchell, J. S. Lundeen, and A. M. Steinberg, Nature **429**, 161 (2004).
[12] T. Nagata, R. Okamoto, J. L. O'Brien, K. Sasaki, and S. Takeuchi, Science **316**, 726 (2007).
[13] K. J. Resch, K. L. Pregnell, R. Prevedel, A. Gilchrist, G. J. Pryde, J. L. O'Brien, and A. G. White, Phys. Rev. Lett. **98**, 223601 (2007).
[14] F. Ferri, D. Magatti, A. Gatti, M. Bache, E. Brambilla, and L. A. Lugiato, Phys. Rev. Lett. **94**, 183602 (2005).
[15] J. Xiong, D.-Z. Cao, F. Huang, H.-G. Li, X.-J. Sun, and K. Wang, Phys. Rev. Lett. **94**, 173601 (2005).
[16] O. Kwon, Y.-W. Cho, and Y.-H. Kim, Phys. Rev. A **78**, 053825 (2008).
[17] C. K. Hong, Z. Y. Ou, and L. Mandel, Phys. Rev. Lett. **59**, 2044 (1987).
[18] O. Kwon, Y.-S. Ra, and Y.-H. Kim, Opt. Express **17**, 13059 (2009).
[19] S.-Y. Baek and Y.-H. Kim, Phys. Rev. A **77**, 043807 (2008).
[20] R. Okamoto, H. F. Hofmann, T. Nagata, J. L. O'Brien, K. Sasaki, and S. Takeuchi, New J. Phys. **10**, 073033 (2008).
[21] C. Santori, D. Fattal, J. Vuckovic, G. S. Solomon, and Y. Yamamoto, Nature **419**, 594 (2002).
[22] P. J. Mosley, J. S. Lundeen, B. J. Smith, P. Wasylczyk, A. B. U'Ren, C. Silberhorn, and I. A. Walmsley, Phys. Rev. Lett. **100**, 133601 (2008).
[23] Y.-H. Kim and W. P. Grice, Opt. Lett. **30**, 908 (2005).
[24] Y.-H. Kim and W. P. Grice, J. Opt. Soc. Am. B **22**, 493 (2005).